Journal of proteome research

Article

pubs.acs.org/jpr

Terms of Use

Quantitative Proteomics Profiling of Primary Lung Adenocarcinoma Tumors Reveals Functional Perturbations in Tumor Metabolism

Maria Pernemalm,*[,†] Luigi De Petris,[‡] Rui M. Branca,[†] Jenny Forshed,[†] Lena Kanter,[‡] Jean-Charles Soria,[§] Philippe Girard,[∥] Pierre Validire,[∥] Yudi Pawitan,[⊥] Joost van den Oord,[#] Vladimir Lazar,[▽] Sven Påhlman,[○] Rolf Lewensohn,[‡] and Janne Lehtiö*[,†]

[†]Cancer Proteomics Mass Spectrometry, Department of Oncology-Pathology, Science for Life Laboratory, Karolinska Institutet, Stockholm, Sweden

[‡]Department of Oncology and Pathology, Karolinska Institutet/Karolinska University Hospital, Stockholm, Sweden

[§]Institut Gustave-Roussy, Villejuif, France, and Université Paris XI, Le Kremlin-Bicêtre, France

[∥]Institut Mutualiste Montsouris, Paris, France

[⊥]Department of Medical Epidemiology and Biostatistics, Karolinska Institutet, Stockholm, Sweden

[#]Translational Cell & Tissue Research, Department of Imaging and Pathology, KU Leuven, Leuven, Belgium

[▽]Unité de Génomique Fonctionnelle et Bioinformatique, Institut Gustave Roussy, Villejuif, France

[○]Center for Molecular Pathology, Department of Laboratory Medicine, CREATE Health, Lund University, Skåne University Hospital, Malmö, Sweden

Supporting Information

ABSTRACT: In this study, we have analyzed human primary lung adenocarcinoma tumors using global mass spectrometry to elucidate the biological mechanisms behind relapse post surgery. In total, we identified over 3000 proteins with high confidence. Supervised multivariate analysis was used to select 132 proteins separating the prognostic groups. Based on in-depth bioinformatics analysis, we hypothesized that the tumors with poor prognosis had a higher glycolytic activity and HIF activation. By measuring the bioenergetic cellular index of the tumors, we could detect a higher dependency of glycolysis among the tumors with poor prognosis. Further, we could also detect an up-regulation of HIF1α mRNA expression in tumors with early relapse. Finally, we selected three proteins that were upregulated in the poor prognosis group (cathepsin D, ENO1, and VDAC1) to confirm that the proteins indeed originated from the tumor and not from a stromal or inflammatory component. Overall, these findings show how in-depth analysis of clinical material can lead to an increased understanding of the molecular mechanisms behind tumor progression.

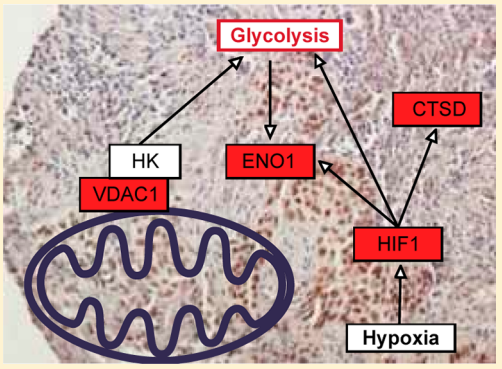

KEYWORDS: *NSCLC, adenocarcinoma, relapse, glycolysis, hypoxia, HIF1, ENO1, VDAC1, CTSD, Warburg, prognosis, peptide isoelectric focusing*

INTRODUCTION

Lung cancer is the primary cause of cancer-related death worldwide, leading to an estimated 1.4 million deaths in 2010 according to the World Health Organization (www.who.int/mediacenter/factsheets/fs297/en/). Despite major efforts to improve the therapy in nonsmall cell lung cancer (NSCLC), few breakthroughs have been made for the overall patient population. In early stage NSCLC, surgery and, to some extent, radiotherapy are curative treatments. However, despite the curative intent, approximately 50% of all patients will relapse post surgery.[1] In patients with advanced disease, platinum-based chemotherapy is still the most common therapy. However, resistance to therapy is common, resulting in an overall 5-year survival rate of approximately 15% in the entire lung cancer patient population.[2]

Recently, several high profile publications on whole genome sequencing and RNA sequencing of NSCLC have been published.[3−7] These studies have provided important insight into the diverse genomic landscape of NSCLC and highlighted the complexity, tumor heterogeneity and high mutagenic rate of this disease. However, these studies have primarily focused on detecting novel driver mutations and therapeutic targets in NSCLC rather than discovering mechanisms coupled to prognosis or response to treatment. In addition, none of the

Received: March 7, 2013
Published: July 31, 2013

Table 1. Clinical Data Summary of the 16 Tumor Samples[a]

patient ID	age at diagnosis	gender (M/F)	smoker[b]	histology	pT(TNM)	pN(TNM)	pM(TNM)	% cancer cells	follow up (years)	relapse (Y/N)	status[c]
127	76	F	1	AC	2	0	0	65	3.5	N	0
140	55	M	2	AC	2		1	95	4.2	N	0
412	63	M	1	SCC	2	1	0	80	5.4	N	1
541	50	F	1	AC	1	1	0	80	2.3	N	1
344	56	M	2	AC	3	1	0	70	4.5	N	1
225	58	F	1	AC	2	2	0	80	3.3	N	1
278	49	M	1	AC	2	2	0	90	6.3	N	1
118	69	F	1	AC	2	0	0	100	1	Y	1
146	57	M	2	AC	4	1	0	100	2.9	Y	0
210	62	F	2	AC	1	2	0	95	2.6	Y	0
255	59	M	2	AC	2	2	0	50	5.3	Y	1
295	77	F	2	AC	2	0	0	100	0.9	Y	0
322	62	M	2	AC	2	2	0	90	4.6	Y	1
396	57	M	1	AC	2	0	0	80	1.5	Y	0
247	58	F	1	AC				100	2.5	Y	1
421	49	F	1	AC	1	2	0	90	1.6	Y	0

[a]M = male, F = female, AC = adenocarcinoma, SCC = squamous cell carcinoma, pT(TNM) = tumour size as defined by pathologist examination of the surgical specimen according to the TNM classification of malignant tumours, pN(TNM) = degree of spread to regional nodes as defined by pathologist examination of the surgical specimen according to the TNM classification, pM(TNM) = presence of distal metastasis according to the TNM classification, follow up (years) = years post date of surgery. [b]1 = current, 2 = former. [c]0 = dead, 1 = alive.

studies have investigated the phenotypic landscape in terms of global protein expression. Kikuchi et al recently published the first in-depth proteomics analysis of primary tumor material from NSCLC. Using a combination of peptide isoelectric focusing and shotgun mass spectrometry, they identified 3621 proteins from pooled samples, being the highest number of proteins detected from NSCLC to date.[8] The study aimed at detecting novel proteins for early diagnosis as well as novel activated pathways in lung cancer. Indeed, they identified both diagnostic proteins discriminating between squamous cell carcinoma and adenocarcinoma, as well as a novel group of kinases (p21-activated kinases, PAKs) important for lung tumorigenesis, highlighting the potential of global proteomics analysis of tumor material from NSCLC.

The aim of the current study is to discover novel mechanisms predictive of relapse post surgery in lung adenocarcinoma by in-depth proteomics analysis. Using narrow range peptide isoelectric focusing and global mass spectrometry, we have analyzed lung adenocarcinoma tumors from 9 patients with relapse within 2 years after surgery and from 7 patients with no relapse within 2 years after surgery.

To analyze the proteomics data, we have used both univariate and multivariate statistics as well as pathway analysis. Selected findings have been explored in detail by functional assays, mRNA expression levels, and immunohistochemistry.

The results from this study have implications in understanding progression and tumor metabolism in lung adenocarcinoma and for assessment of prognosis and potential therapy guidance in nonsmall cell lung cancer. Determining the molecular factors underlying tumor recurrence of this malignancy is of outmost importance to develop future therapeutic interventions and improve the survival of this group of patients.

EXPERIMENTAL PROCEDURES

Tumor Samples

Nonsmall cell lung cancer patients underwent surgical resection in a single institution (Institut Mutualiste Montsouris in Paris, France) between 2002 and 2006 and signed a consent allowing use of their tumor for research purposes. The ethics committee at the Institute Gustave Roussy approved the current study. Surgical samples where snap frozen and put in −80 °C. From each patient, 40 cryo-sections, each 20 μm thick, were cut and kept in −80 °C until preparation. A pathologist analyzed all surgical specimens, and histology and the percentage of tumor cells in sample were evaluated. Two groups of patients were included in the current study, patients with relapse within 2 years of surgery and patients with no relapse within 2 years of surgery. Samples were further selected based on adenocarcinoma histology, smoking status (nonsmokers were excluded), and tumor cell content (≥50%). The groups were balanced based on age, sex, and smoking status (former/current). A more detailed description of the clinical data can be found in Table 1.

Sample Preparation

A total of 400 μL of lysis buffer containing 4 M urea and 1% CHAPS was added to each of the cryosectioned samples. The sections were mechanically disrupted using a plastic pestle and vortexed several times and subsequently incubated for 30 min on ice. An additional 100 μL of lysis buffer was then added to the samples, which were then vortexed thoroughly. To remove debris, the samples were centrifuged for 10 min in 4 °C 10 000*g*. The supernatant was then taken off, and protein concentration was measured using DC Protein Assay kit (BioRad). From each sample, 160 μg of protein was taken off and precipitated using four volumes of ice-cold acetone. The samples where kept on ice for 1 h and subsequently centrifuged for 10 min in 4 °C 10 000*g*. The supernatant was disregarded and the pellet was allowed to air-dry.

Digestion of Proteins and iTRAQ Labeling

The precipitated samples were dissolved in iTRAQ dissolution buffer and digested overnight according to manufacturer's instructions (Applied Biosystems). Once digested, eight internal standard (IS) were made by pooling 55 μg of each digested sample, and subsequently aliquoting the pooled sample into eight 100 μg aliquots. Second, 100 μg of peptides from each individual sample as well as the eight IS aliquots were

dx.doi.org/10.1021/pr4002096 | J. Proteome Res. 2013, 12, 3934−3943

labeled using iTRAQ labeling as shown in Supporting Information Table 1. In total, three individual iTRAQ pools were created. The pooled iTRAQ labeled digests were then applied to 1 mL Strata X-C 33 μm polymeric strong cation exchange (SCX) microcolumns (Phenomenex). The microcolumns were initially washed with 1 mL of 100% methanol followed by 1 mL of Milli-Q grade water. The sample was adjusted to 500 μL 0.1% formic acid and then applied to the columns. After wash with 1 mL of 30% methanol 0.1% formic acid, the samples were eluted with 30% methanol and 5% ammonium hydroxide. Samples were then dried in a SpeedVac system.

Narrow Range Peptide Isoelectric Focusing

The three pooled iTRAQ labeled samples were dissolved in 150 μL rehydration solution containing 8 M urea, 1% IPG buffer pH 3.5−5.0 (GE Healthcare). Three twenty-four cm 3.7−4.9 linear gradient strips (GE Healthcare) were incubated overnight according to manufacturer's instructions. Samples were applied to IPG strips by gel bridge (pH 3.3) at the cathode end and run as described in.[9] After focusing the strips were cut in 24 pieces. Peptides were then eluted in two steps. First, 240 μL 0.1% trifluoro acetic acid (TFA) was added to each piece from the strip and incubated for 2 h on a shaking board. The liquid was collected and 240 μL 0.1% TFA 50% acetonitrile was added for a second elution step. After 2 h incubation on shaking board the passive elution solution was then collected and pooled with the extracted peptides from the fist elution. Samples were then dried in SpeedVac and kept at −20 °C until analysis. Fractions 1−2, 4−9, and 12−24 were used for mass spectrometry analysis.

LC/MS/MS Analysis

From each IPG fraction 2 μL was injected into online HPLC-MS performed on a hybrid LTQ-Orbitrap Velos mass spectrometer (Thermo Fischer Scientific, San Jose, CA). An Agilent HPLC 1200 system (Agilent) was used to provide the gradient for online reversed-phase nano-LC at a flow of 0.4 μL/min. Solvent A was 97% water, 3% ACN, 0.1% formic acid; and solvent B was 5% water, 95% ACN, 0.1% formic acid. The curved gradient went from 2% B up to 40% B in 45 min, followed by a steep increase to 100% B in 5 min. The sample was injected into a C18 guard desalting column (Agilent) prior to a 15 cm long C18 picofrit column (100 μm internal diameter, 5 μm bead size, Nikkyo Technos Co., Tokyo, Japan) installed on to the nanoelectrospray ionization (NSI) source. Precursors were isolated with a 2 m/z width and dynamic exclusion was used with 60 s duration. We enabled "preview mode" for FTMS master scans, which proceeded at 30 000 resolution (profile mode). Data-dependent MS/MS (centroid mode) followed in two stages: first, the top 5 ions from the master scan were selected for collision induced dissociation (CID, at 35% energy) with detection in the ion trap (ITMS); and after, the same 5 ions underwent higher energy collision dissociation (HCD, at 45% energy) with detection in the orbitrap (FTMS). The entire duty cycle lasted ∼3.5 s.

The .raw files from the Orbitrap analysis were searched by Sequest under the software platform Proteome Discoverer 1.3.0.339 (Thermo) against the Ensemble human protein sequence database (homosapiens.GRCh37.63.pep.all.fasta containing 76 501 entries) using a 99% confidence cutoff limit and using percolator[10,11] version 1.17 (2010-11-30) for false discovery rate cutoff. A precursor mass tolerance of 10 ppm, and product mass tolerances of 0.02 Da for HCD-FTMS and 0.8 Da for CID-ITMS were used. Further settings used were trypsin with 1 missed cleavage; MMTS on cysteine and iTRAQ8plex on lysine and N-terminal as fixed modifications; oxidation of methionine and phosphorylation of serine, threonine, or tyrosine as variable modifications. Probabilities for phosphosite localization (within each phosphopeptide) were calculated using the phosphoRS node of Proteome Discoverer. Quantitation of iTRAQ8plex reporter ions was done by Proteome Discoverer on HCD-FTMS tandem mass spectra using an integration window tolerance of 20 ppm. The pooled internal standards were used as denominators in the iTRAQ quantification to enable quantitative comparison between the three iTRAQ pools (Supporting Information Table 1 listing iTRAQ pooling scheme and file listing all peptides). We used the MAYU algorithm[12] to identify peptide score limits corresponding to the protein confidence false discovery rate (FDR) .

Statistical Analysis, Protein Annotation, and Pathway Analysis

The univariate analysis (Student's t test) and the survival analysis (mantel-cox test) were performed using GraphPad Prism 5.0 (GraphPad Software Inc.). Multivariate statistics and modeling was performed with SIMCA (SIMCA-P+ 12.0, Umetrics, Sweden).[13] The multivariate analysis was performed on mean centered, unit variance scaled data, assuming equal importance of each protein. Orthogonal partial least-squares (OPLS) was used to build classification models. For optimization of OPLS models we used VIP (Variable Importance in projection) value[14] to judge protein importance in the model. The OPLS models were validated by 7-fold cross validation. Proteins with significant VIP throughout the cross validation of the model were selected for the optimized model. CV-ANOVA was used to judge the model validity.

Clustering and gene ontology enrichment analysis of the 132 proteins from the OPLS model was performed using Babelomics 4.3 (http://babelomics.bioinfo.cipf.es/).[15] The clustering was performed using an unsupervised self-organizing tree algorithm (SOTA).[16] Individual clusters were analyzed for gene ontology term enrichment (biological process and molecular function) using the all proteins detected in the experiment as background.

For pathway analysis and functional classification, Ingenuity Pathway Analysis (Ingenuity pathway analysis, IPA, www.ingenuity.com) was used. In brief, Ingenuity uses Fischer's exact test to calculate the probability that a set of proteins is associated to a pathway by chance.

Assessment of Tumor Metabolism

The bioenergetic cellular index (BEC-index) was developed to measure cells use of glycolysis in relation to the use of the mitochondrial respiratory chain/oxidative phosphorylation.[17] Same samples as analyzed on the proteomics platform were also analyzed in the BEC experiment, essentially as described in ref 18. Due to lack of remaining material, three samples had to be excluded in this analysis (sample s118, 278, and 322); in addition, the outliers (146 and 255) and the squamous sample (412) were excluded. For the remaining 10 samples, whole-cell lysates were subjected to gel electrophoresis and blotted onto polyvinylidene difluoride membranes. Anti-GAPDH antibody (1:1000 Cell Signaling Technology), anti-Hsp60 antibody (1:1000; Abcam), and anti-β-ATPase (1:250 Atlas antibodies) were used for protein detection. Quantification was done using

dx.doi.org/10.1021/pr4002096 | J. Proteome Res. 2013, 12, 3934−3943

SuperPico developing agent and FUJI LAS-1000 as previously described.

mRNA Expression Analysis

The following 14 tumor samples from the original cohort were analyzed on exon array: 146, 210, 322, 118, 255, 295, 396, 127, 140, 541, 278, 225, and 344. Briefly, the exon array is the 244K array from Agilent, with a custom design of around 195 000 probes (60-mers) of exons of around 19 500 genes (hg18 refGene.txt from UCSC). Scanning was performed using Agilent G2565C microarray scanner.

Immunohistochemistry

The three proteins selected in the OPLS analysis were validated on tissue microarray comprised of 100 primary NSCLC samples. Patients were selected on the basis of the availability of formalin-fixed and paraffin-embedded tumor tissue. Primary tumors were resected at Karolinska University Hospital between 1987 and 1992. The ethical committee at Karolinska Hospital approved the study. Major patient and tumor characteristics were as follows: female 61%, median age (range) 68 years (41−82), tumor stage IA/IB 38%/62%, tumor grading G1/G2/G3 20%/38%/42%, tumor histology squamous/nonsquamous 52%/48%. Median overall survival (interquartile range) was 54 months (25−111 months). At time of analysis 17 patients were alive and censored at last follow-up date. Median follow up time in living cases was 65 months.[19] The following primary antibodies were used: VDAC1 (Abcam ab15895), cathepsin D (SantaCruz sc-10725), and ENO1 (SantaCruz sc-15343).

Briefly, tissue sections were deparaffinized and rehydrated through graded ethanol to deionized water. Antigen retrieval was performed with sodium citrate buffer at pH 6 in microwave for 20 min, and the endogenous peroxidase activity was blocked by hydrogen peroxide, 0.5% for 30 min. Sections were incubated overnight with the primary rabbit polyclonal or mouse monoclonal antibodies listed above. Biotinylated horse anti-mouse and goat anti-rabbit IgG were used as secondary antibody, as appropriate. The third step comprised application of avidin−biotin-peroxidase complex. The peroxidase reaction was developed using 3,3-diaminobenzidine (DAB) for 6 min. IHC stainings were evaluated by a pathologist. HIF1α staining was obtained with an automated method performed as in ref 20. IHC stainings were evaluated by applying a semiquantitative method. The immunoreactivity of the sample was determined by the percentage of positive cells: 1 point for <25%, 2 points for 25−50%, 3 points for 50−75% of cells, and 4 points for >75% of cells. In addition, the intensity of staining was graded as follows: grade 0 (negative), 1 (weak), 2 (moderate), and 3 (strong). The total score for each case was obtained as the product of intensity of staining and percentage of cells stained. Given the semiquantitative nature of IHC as an experimental method to determine protein expression on tissue, each protein was considered low-negative expressed vs high-positive expressed applying the following cutoffs based on IHC total scores (intensity x percentage of stained cells). VDAC1 was considered low-negative if scored 0 to 4 and high-positive if scored 6 to 12. Cathepsin D and HIF1α were considered low-negative if scored 0 to 3 and high-positive if scored 4 to 12. For each protein the cutoff was chosen on the basis of the number and statistical significance in terms of associations between proteins and clinical correlates.

RESULTS

The tumor samples were lysed, digested, iTRAQ labeled, and applied to narrow range peptide isoelectric focusing (IEF) and subsequent mass spectrometry analysis. A summary of the clinical characteristics of the samples can be found in Table 1.

To enable quantification across all samples and for reproducibility calculations we used pooled internal standards in each iTRAQ run (made up by all the individual samples in the study).

In total we identified 3146 proteins using a one peptide 1% significance cut off limit (the protein data and corresponding peptide data can be found in the Supporting Information). Out of these proteins, 1461 were detected and quantified across all 16 samples with at least one unique peptide (86%, >1 unique peptide). Using MAYU, we defined the protein FDR; 1409 of the 1461 proteins had protein FDR below 5%. Only these 1409 proteins were used in the downstream differential analysis (Supporting Information). Among the 1409 proteins, we detected several proteins known to be important in lung cancer tumorigenesis including AKT, ERK, EGFR, STAT3, and PKC.

Secondary pathological evaluation of the specimens revealed that one patient (patient number 412) was initially misclassified as adenocarcinoma and was truly of squamous cell carcinoma histology. Analyzing the proteomics data, we could also detect a correlation with expected squamous cell carcinoma markers in this sample, such as low levels of cytokeratin 7 and very high levels of cytokeratin 5 (Figure 1). Based on this misclassification, sample 412 was removed from the study cohort and not included in the downstream statistical analysis.

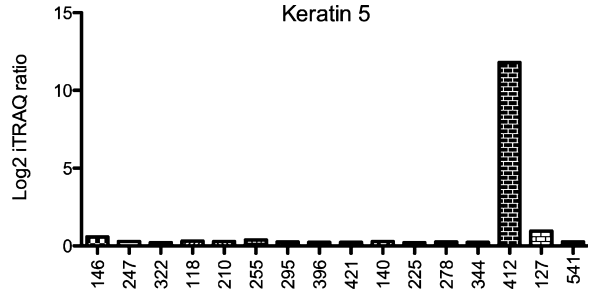

Figure 1. Keratin 5 protein expression among all patients. Log2 iTRAQ ratio on the *y*-axis, and sample number on the *x*-axis.

Outlier Detection

As a part of the quality control of the proteomics data we did outlier detection and subgroup analysis using principle component analysis (PCA) (Figure 2). The internal standards clustered tightly in the center of the PCA plot, indicating high reproducibility within and between the different iTRAQ experiments. This was confirmed by calculating the standard deviation of the iTRAQ intensities between the pooled internal standards, resulting in a standard deviation of 0.007. No subgroups were evident among the patients; however, two outliers were detected, patient 146 and patient 255 (defined as outside the Hotelling's ellipse, significance level 0.05) (Figure 2). An in-depth analysis of the two outliers can be found in the Supporting Information. In brief, sample 255 showed high plasma protein contamination, and in addition this sample had the lowest tumor cell content among the samples included in this study (50%). Sample 146 on the other hand showed a very high degree of genetic instability, which greatly affected the

dx.doi.org/10.1021/pr4002096 | J. Proteome Res. 2013, 12, 3934−3943

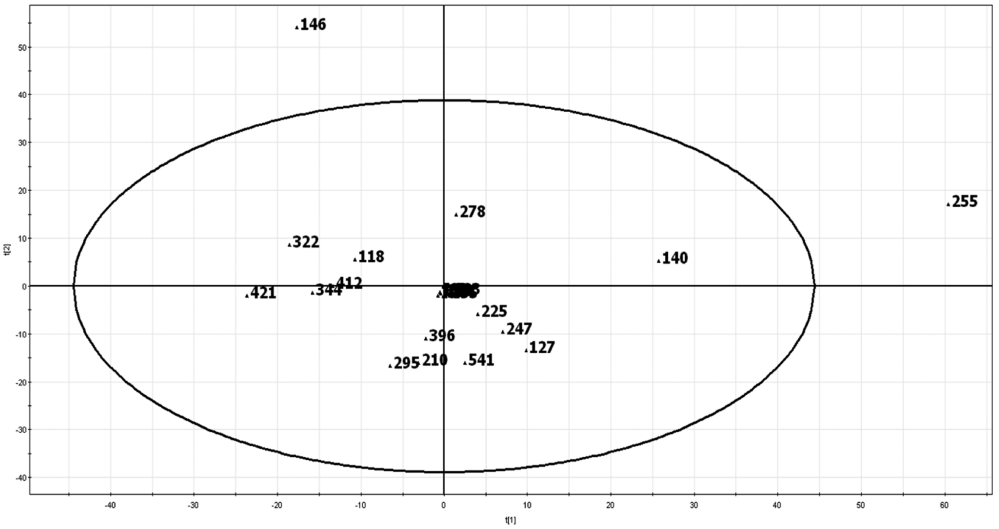

Figure 2. Principle component analysis (PCA) of the 16 samples and the 8 pooled internal standards, based on all 1461 proteins with quantitation from the mass spectrometry analysis.

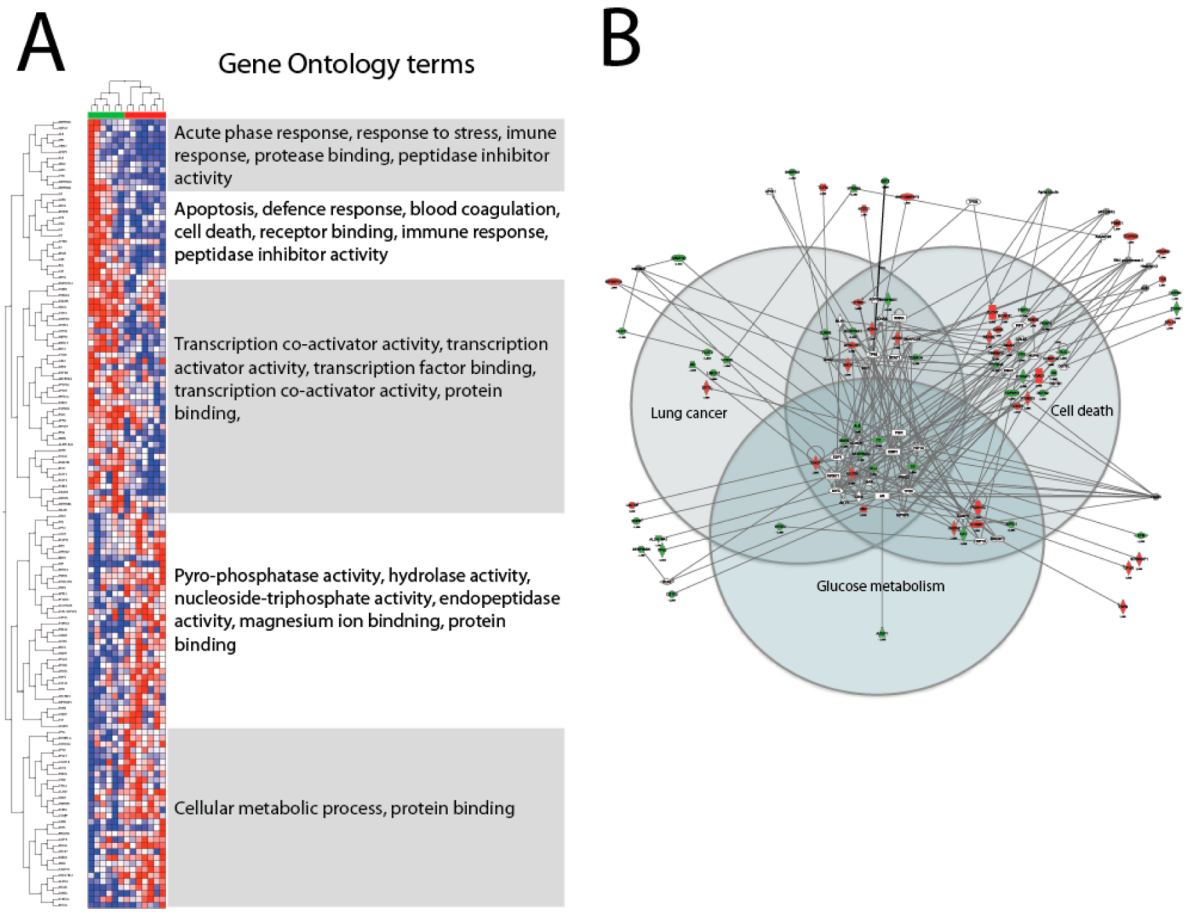

Figure 3. (A) Clustering of the samples and the 132 proteins from the OPLS model. Samples with no relapse indicated in the top of the dendrogram in green and samples with relapse in red. Protein clusters and corresponding representative enriched GO terms are shown to the right. A detailed list of the proteins and all GO terms in each cluster can be found in the Supporting Information. (B) Protein network based on IPA network analysis of the 132 proteins from the OPLS model. Only proteins with a direct relationship to any of the proteins in the OPLS model are included in the network (indicated in white). Upregulated proteins in relapse are shown in red and downregulated in green. The network is arranged as a Venn diagram based on functional classification. Proteins coupled to cell death (IPA terms: cell death, cell death of epithelial cells, cell death of tumor cells, cell death of epithelial cell lines, and cell death of lung cancer cell lines), lung cancer (IPA terms: lung tumor, NSCLC ,and lung cancer), and glycolysis (IPA terms: glycolysis of cells, glycolysis, internalization of carbohydrates, quantity of carbohydrates, concentration of glucose, and glucose metabolism disorder) are included in the Venn diagram. Proteins outside Venn diagram are not coupled to any of the three functional categories.

dx.doi.org/10.1021/pr4002096 | J. Proteome Res. 2013, 12, 3934−3943

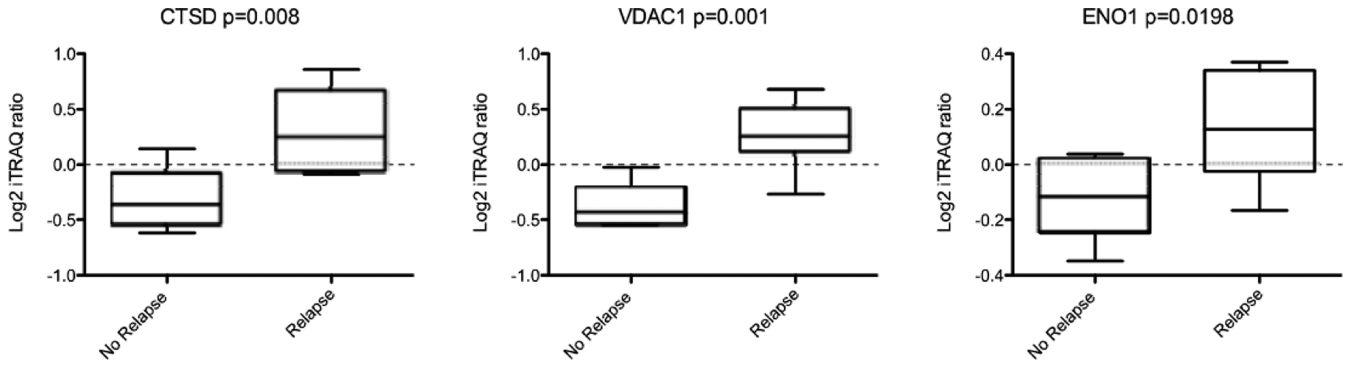

Figure 4. Box plots showing the log2 iTRAQ ratios of the three proteins selected for validation. *p*-Value based on Student's *t* test.

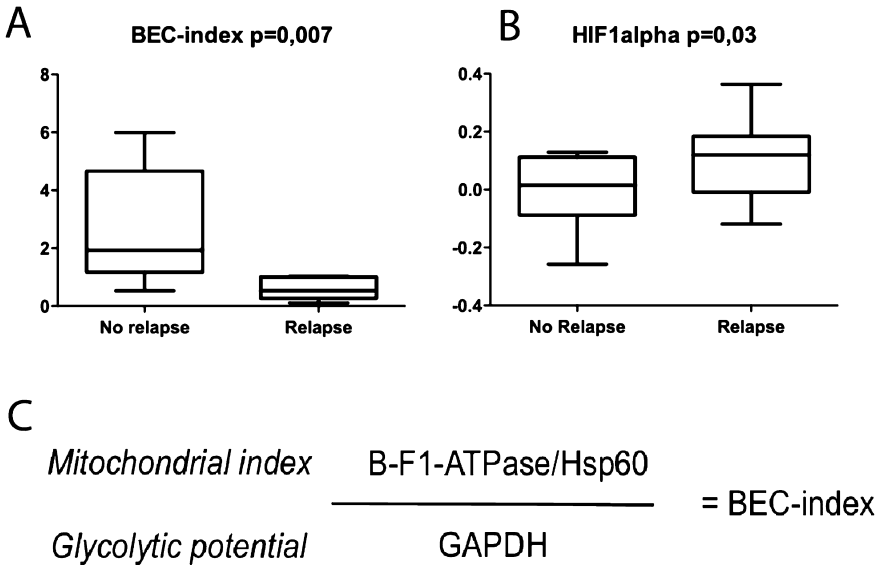

Figure 5. (A) Bioenergetic cellular index, BEC-index, indicating higher glycolytic activity in tumor tissue from relapse cases. BEC-index on *y*-axis. *p*-Value based on Student's *t* test. (B) Boxplot showing log2 mRNA expression of HIF1*α*. (C) Theoretical summary of the BEC-index.

overall proteome, transcriptome, and genome in this sample. Based on the outlier analysis, we decided to remove samples 146 and 255 from the differential analysis as they introduced unmatched biological and/or sample preparation variability that would skew the downstream statistical analysis.

Differential Analysis

We pursued two separate approaches to analyze the differences in molecular phenotype between the two groups; a hypothesis generating functional *pathway analysis* approach based on multivariate data analysis and a *target verification* approach based on univariate data analysis. For the multivariate data analysis we employed Orthogonal Partial Least Square (OPLS), and for the univariate analysis we used *t* test statistics.

Proteome Changes Related to Relapse. Using OPLS, we created a model that was able to separate the relapse and nonrelapse group based on 132 proteins, with a *p*-value of 0.001 and a good predictive value (Q^2 = 0.75) (Supporting Information Table 2). The OPLS model included a broad spectrum of proteins: enzymes (30%), transport proteins (9%), peptidases (8%), transcription regulators (7%), translation regulators (2%), phosphatases (2%), kinases (2%), ion channels (2%), transmembrane proteins (1%), and other/unknown proteins (38%) as defined by Ingenuity pathway analysis (IPA). To identify possible correlations between the proteins within the OPLS model, we performed a self-organizing tree algorithm (SOTA) clustering analysis of the 132 proteins. The individual clusters were subsequently analyzed by gene ontology analysis. Among the clusters with a high expression in the nonrelapse group, we found a significant enrichment of terms related to immune response and cell death, whereas among clusters with a high expression in the relapse group we found an enrichment of terms related to metabolic activity. Representative GO terms for each cluster are shown in Figure 3A. A detailed list of the proteins and the enriched GO terms in each cluster can be found in the Supporting Information. To further pinpoint the underlying biological functions causing the relapse, we performed pathway enrichment analysis based on the 132 proteins using IPA. Among the top 10 significantly enriched pathways, we found several pathways related to glucose metabolism including: glycolysis (p = 0.001), gluconeogenesis (p = 0.001), and pentose phosphate pathway (p = 0.002).

Network analysis of the OPLS proteins using IPA revealed connections to HIF1alpha in a network containing 77 of the 132 molecules (Supporting Information). The top functions in this network (as defined by IPA) were cancer and respiratory disease. In particular a large number of the proteins in the network were associated to subcategories related to cell death (IPA terms: cell death, cell death of epithelial cells, cell death of tumor cells, cell death of epithelial cell lines, and cell death of lung cancer cell lines), lung cancer (IPA terms: lung tumor,

dx.doi.org/10.1021/pr4002096 | J. Proteome Res. 2013, 12, 3934−3943

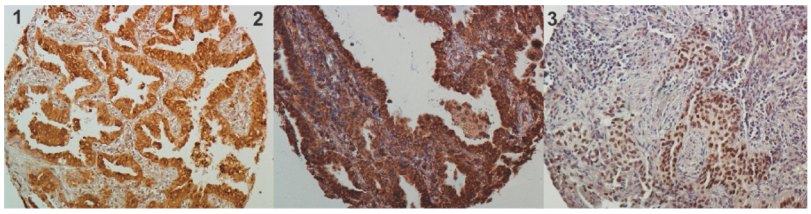

Figure 6. Immunohistochemistry slides showing representative staining of (1) CTSD, (2) VDAC1, and (3) HIF1α in independent primary lung adenocarcinoma samples.

NSCLC, and lung cancer), and glycolysis (IPA terms: glycolysis of cells, glycolysis, internalization of carbohydrates, quantity of carbohydrates, concentration of glucose, and glucose metabolism disorder) as illustrated in Figure 3B.

In the univariate analysis, we detected 72 proteins with a p-value <0.05 (Supporting Information Table 3). A comparison of the proteins from the OPLS model and the *t* test showed that all the significant proteins from the *t* test were also included in the OPLS model.

To prioritize and reduce the number of proteins for verification, we refined the OPLS model. Based on high VIP score, low *p*-value from the *t* test, and upregulation in poor prognosis, we selected three proteins (VDAC1, CTSD, and ENO1) and made a new OPLS model. Based on only three proteins, we could create a model with a *p*-value of 0.01 and a Q^2 of 0.61. These three proteins were chosen for validation using immunohistochemistry. Protein abundance levels of the protein panel members can be seen in Figure 4.

Validation

Analysis of Metabolic Status. Based on the bioinformatics analysis, we hypothesized that the patients with poor prognosis had a higher glycolytic activity. To test this, we measured the Bioenergetic cellular index (BEC-index) in the tumor samples. The BEC-index was developed to measure cellular use of glycolysis in relation to the use of the mitochondrial respiratory chain/oxidative phosphorylation.[17] The index compares the mitochondrial bioactivity index with the cellular glycolytic potential (Figure 5). The mitochondrial index consists of the ratio of protein levels of the beta-catalytic subunit of the H^+-ATP synthase (β-F1-ATPase) to the mitochondrial chaperone protein Hsp60. β-F1-ATPase is a mitochondrial ATP synthase that utilizes an inner membrane electrochemical gradient to catalyze the synthesis of ATP during oxidative phosphorylation. An inverse correlation between levels of β-F1-ATPase and aerobic glycolysis has previously been shown.[21] The glycolytic potential is represented by protein levels of GAPDH, which is an enzyme that catalyzes an important energy-yielding step in the glycolysis, the reversible oxidative phosphorylation of glyceraldehyde-3-phosphate. In this study, the relapse group had a significantly lower BEC-index ($p = 0.007$) than the no relapse group, which confirms our hypothesis of a higher glycolytic activity among the relapse patients.

HIF1α Expression. The network analysis showed that several of the proteins in the OPLS model were coupled to HIF1α. In addition, literature search showed that both CTSD and ENO1 were known to be induced by transcription factor HIF1. HIF1 regulates cells response to hypoxia and induces metabolic changes in the cell. To further explore mechanisms underlying the increased glycolytic activity in patients with poor prognosis we chose to investigate the mRNA expression HIF1α, which is the oxygen sensitive and regulated subunit of HIF1. HIF1α was under the detection limit of the global proteomics analysis and hence it was evaluated on mRNA level. Indeed, the HIF1α mRNA expression was significantly upregulated among the relapse patients compared to the no relapse patients (Figure 5B).

Immunohistochemistry. To validate that the detected proteins originated from the tumor cells and not from a stromal or inflammatory component, we performed immunohistochemistry (IHC) and stained for VDAC1, CSTD, HIF1α, and ENO1 in lung adenocarcinoma tissue. Out of the four proteins, we succeeded in setting up IHC for all proteins except for ENO1. Representative positive staining for each of the antibodies can be found in Figure 6. As seen in Figure 6, all proteins were expressed in the tumor cells. In addition, all of them, except HIF1α, were expressed in the cytoplasm. HIF1α was detected in the nucleus and showed a patchy pattern, being more strongly expressed in tumor areas surrounding necrosis. VDAC on the other hand showed a characteristic granulated pattern. The percentage of positive cases of each protein (out of the number of successfully evaluated cases in the NSCLC cohort) was as follows: cathepsin D 55% ($n = 82$), VDAC1 45% ($n = 82$), and HIF1α 26% ($n = 94$). No data was available on relapse in this cohort; however, we used quantitative information from the IHC to explore the correlation between the three proteins. A summary of the correlation analysis can be found in Table 2 and Figure 7. In this small cohort, none of the proteins showed any correlation with overall survival.

Table 2. Correlations between the Expression Levels of the Individual Proteins in the Immunohistochemistry Analysis[a]

	cathepsin	VDAC1	HIF1α
cathepsin	×××	Dir p = 0.04	Dir=p0.01
VDAC1	Dir p = 0.04	×××	
HIF1α	Dir=p0.01		×××
histology	$p = 0.04$[b]		

[a]Dir = Direct association. [b]Proteins are more strongly expressed in nonsquamous tumors than in squamous.

■ DISCUSSION

The aim of this study was to discover biological mechanisms behind a poor prognosis post surgery in lung adenocarcinoma. Sixteen primary lung adenocarcinoma tumors were analyzed using mass spectrometry based proteomics. In total, over 3000 proteins were identified. By multivariate analysis, a discriminant model was created that could separate the relapse group and from the nonrelapse group. Using gene ontology enrichment and pathway analysis an enrichment of proteins related to cell metabolism and glycolysis was detected.

It has long been recognized that tumor cells have an altered metabolism compared with normal cells. While normal cells

dx.doi.org/10.1021/pr4002096 | J. Proteome Res. 2013, 12, 3934−3943

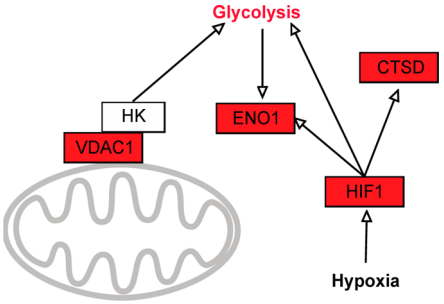

Figure 7. Summary of the findings from the current study. ENO1, CTSD, and VDAC1 were found to be upregulated among the relapse patients in the proteomics analysis. HIF1α was upregulated on mRNA level, and the BEC index indicated a higher glycolytic activity in the patients with relapse. HK = hexokinase.

produce more than 90% of their ATP via oxidative phosphorylation in the mitochondria, tumor cells are known to have increased glucose consumption and lactate production, alongside a decrease in O_2 dependent oxidative phosphorylation. This results in dependence of glucose for ATP production in the tumor cells, while intermediate products from the glycolysis, as well as lipids and amino acids, are redirected for use in anabolic synthesis.[22,23] The shift toward glycolysis allows cells to grow faster than if they used most of the glucose to produce ATP through respiration.

To confirm the hypothesis that the tumors with poor prognosis had a higher dependency on glycolysis, we measured the Bioenergetic cellular index (BEC-index) in the tumor samples. This analysis showed a lower BEC index among relapse patients, indicating that the relapse patients had highly glycolytic tumors. Low BEC-index has previously been shown to correlate with poor prognosis in 90 lung adenocarcinomas and 10 uninvolved lung tissue samples,[24] supporting our findings. However, no molecular mechanism was explored to pinpoint the underlying factors causing this highly glycolytic phenotype in that study.

The transcription factor HIF1 is one of the important players in modulation of cell metabolism and plays an essential role in cellular and systemic homeostatic responses to hypoxia. HIF1α in itself induces expression of several glycolytic enzymes, as well as inhibits entry into the TCA-cycle.[25] High tumor expression HIF1α has been shown to correlate with a short survival in NSCLC in several studies.[26−28] In this study we found an increased expression of HIF1α mRNA among the patients with early relapse.

In addition to induction of expression of glycolytic enzymes, HIF1α has also been shown to induce expression of Cathepsin D, which was found to be upregulated in the relapse patients in this study.[29,30] In the IHC analysis we could also detect a significant correlation between the level of HIF1α and cathepsin D in early stage NSCLC. Cathepsin D is an aspartic protease which is localized in acidic lysosomes under normal conditions.[31] The acidic environment in hypoxic tumors is thought to favor the enzymatic activity of cathepsin D, and many cancer cells secrete pro-cathepsin D to the extracellular space, which has been shown to promote invasion and metastasis.[32−35] Cathepsin D has previously been shown to correlate with a poor prognosis in lung adenocarcinoma.[36] Based on the IHC we detected an overall correlation between expression of cathepsin D and nonsquamous histology.

ENO1 (α-enolase) is also known to be upregulated by HIF1α in response to hypoxia.[37] Increase in ENO1 has a direct coupling to glycolytic activity, as the enzymatic role of ENO1 is to convert 2-phosphoglycerate to phosphoenolpyruvate, a hydrolytic reaction in glycolysis. Despite several attempts we did not get reliable results on ENO1 immunohistochemistry, however a metaanalysis of gene-expression and expressed sequence tags (ESTs) has shown that ENO1 is overexpressed in up to 50% of the 24 investigated cancer classes, among them lung cancer.[38]

VDAC1 is a membrane pore protein first found in the mitochondria, where it regulates the energy balance of the mitochondria, as well as of the entire cell, by enabling metabolite (ADP/ATP, succinate, citrate, etc.) exchange between the mitochondria and the cytoplasm.[39] Expression of a truncated active form of VDAC1 in lung cancer has been shown to associate with hypoxic cell survival and correlate with chemotherapy resistance.[40] In addition, VDAC1 has been shown to hamper the glycolytic enzyme hexokinase at the mitochondrial membrane resulting in an increased glycolytic activity by reduction of the inhibition of the enzyme.[41] Hexokinase has several other cancer promoting functions such as being antiapoptotic, and both small molecules and synthetic peptides have been designed to interrupt the interaction between VDAC1 and hexokinase, showing promising results in vitro.[42] In the immunohistochemistry analysis none of the selected proteins showed any correlation with overall survival. Despite not being the primary endpoint in the initial discovery study, this is somewhat disappointing, as relapse and overall survival are closely linked. The lack of correlation could be due to several reasons, both due to analytical differences between the discovery experiment and the validation experiment, as well as due to differences in the two cohorts (the validation cohort being only stage I tumors for example). Additional work is needed to pinpoint these proteins role in tumor metabolism and tumor progression.

Recently, there has been a renewed interest to target the tumor metabolism in oncology. Several novel treatment approaches have emerged as a result of research in the field of tumor metabolism, such as the use of the diabetes drug Metformin to treat cancers,[43] or to combine cytotoxic drugs with short fasting cycles to selectively enhance the treatment effect of traditional chemotherapy in the tumor.[44] Other approaches include targeting the mechanisms in the interplay between glycolytic activity and hypoxia, as this would increase the tumor specificity of the treatment.[45]

As the vast majority of data in this field are based on mouse or cell line studies, our findings provide important evidence that this metabolic shift is also present in vivo in lung adenocarcinoma tumors. In summary, this study shows a functional coupling between high glycolytic activity and relapse post surgery in primary lung adenocarcinoma tumors. In the future, the protein level changes detected in this study could provide a starting point in an attempt to discover predictive markers for metabolic treatment options in lung adenocarcinoma.

■ ASSOCIATED CONTENT

Supporting Information

Additonal files containing information on the following: all proteins, all peptides, overlapping proteins only and protein FDR, PCA outlier analysis, SOTA clusters and GO analysis,

dx.doi.org/10.1021/pr4002096 | J. Proteome Res. 2013, 12, 3934−3943

proteins in network, Table 1 with iTRAQ pooling scheme, Table 2 listing proteins in OPLS model, and Table 3 listing proteins from *t* test. This material is available free of charge via the Internet at http://pubs.acs.org.

AUTHOR INFORMATION

Corresponding Author

*(M.P.) E-mail: maria.pernemalm@ki.se. Telephone: +46703030465. (J.L.) E-mail: janne.lehtio@ki.se. Telephone: +46739789102.

Notes

The authors declare no competing financial interest.

ACKNOWLEDGMENTS

This study was supported by grants from Swedish Cancer Society (Cancerfonden), Stockholm's Cancer Society (Radiumhemmets Forskningsfonder), The European Commission (FP6 Chemores Project, FP7 GlycoHit), and Swedish Research C (VR)

REFERENCES

(1) Goldstraw, P.; Crowley, J.; Chansky, K.; Giroux, D. J.; Groome, P. A.; Rami-Porta, R.; Postmus, P. E.; Rusch, V.; Sobin, L.; Committee, I. A. f. t. S. o. L. C. I. S.; Institutions, P.. The IASLC Lung Cancer Staging Project: proposals for the revision of the TNM stage groupings in the forthcoming (seventh) edition of the TNM Classification of malignant tumours. *J. Thorac. Oncol.* **2007**, *2* (8), 706−714.

(2) Jemal, A.; Siegel, R.; Ward, E.; Hao, Y.; Xu, J.; Thun, M. J. Cancer statistics, 2009. *Ca-Cancer J. Clin.* **2009**, *59* (4), 225−249.

(3) Djebali, S.; Davis, C. A.; Merkel, A.; Dobin, A.; Lassmann, T.; Mortazavi, A.; Tanzer, A.; Lagarde, J.; Lin, W.; Schlesinger, F.; Xue, C.; Marinov, G. K.; Khatun, J.; Williams, B. A.; Zaleski, C.; Rozowsky, J.; Röder, M.; Kokocinski, F.; Abdelhamid, R. F.; Alioto, T.; Antoshechkin, I.; Baer, M. T.; Bar, N. S.; Batut, P.; Bell, K.; Bell, I.; Chakrabortty, S.; Chen, X.; Chrast, J.; Curado, J.; Derrien, T.; Drenkow, J.; Dumais, E.; Dumais, J.; Duttagupta, R.; Falconnet, E.; Fastuca, M.; Fejes-Toth, K.; Ferreira, P.; Foissac, S.; Fullwood, M. J.; Gao, H.; Gonzalez, D.; Gordon, A.; Gunawardena, H.; Howald, C.; Jha, S.; Johnson, R.; Kapranov, P.; King, B.; Kingswood, C.; Luo, O. J.; Park, E.; Persaud, K.; Preall, J. B.; Ribeca, P.; Risk, B.; Robyr, D.; Sammeth, M.; Schaffer, L.; See, L. H.; Shahab, A.; Skancke, J.; Suzuki, A. M.; Takahashi, H.; Tilgner, H.; Trout, D.; Walters, N.; Wang, H.; Wrobel, J.; Yu, Y.; Ruan, X.; Hayashizaki, Y.; Harrow, J.; Gerstein, M.; Hubbard, T.; Reymond, A.; Antonarakis, S. E.; Hannon, G.; Giddings, M. C.; Ruan, Y.; Wold, B.; Carninci, P.; Guigó, R.; Gingeras, T. R. Landscape of transcription in human cells. *Nature* **2012**, *489* (7414), 101−108.

(4) Govindan, R.; Ding, L.; Griffith, M.; Subramanian, J.; Dees, N. D.; Kanchi, K. L.; Maher, C. A.; Fulton, R.; Fulton, L.; Wallis, J.; Chen, K.; Walker, J.; McDonald, S.; Bose, R.; Ornitz, D.; Xiong, D.; You, M.; Dooling, D. J.; Watson, M.; Mardis, E. R.; Wilson, R. K. Genomic landscape of non-small cell lung cancer in smokers and never-smokers. *Cell* **2012**, *150* (6), 1121−1134.

(5) Seo, J. S.; Ju, Y. S.; Lee, W. C.; Shin, J. Y.; Lee, J. K.; Bleazard, T.; Lee, J.; Jung, Y. J.; Kim, J. O.; Yu, S. B.; Kim, J.; Lee, E. R.; Kang, C. H.; Park, I. K.; Rhee, H.; Lee, S. H.; Kim, J. I.; Kang, J. H.; Kim, Y. T. The transcriptional landscape and mutational profile of lung adenocarcinoma. *Genome Res.* **2012**, *22*, 2109−2119.

(6) Imielinski, M.; Berger, A. H.; Hlammerman, P. S.; Hernandez, B.; Pugh, T. J.; Hodis, E.; Cho, J.; Suh, J.; Capelletti, M.; Sivachenko, A.; Sougnez, C.; Auclair, D.; Lawrence, M. S.; Stojanov, P.; Cibulskis, K.; Choi, K.; de Waal, L.; Sharifnia, T.; Brooks, A.; Greulich, H.; Banerji, S.; Zander, T.; Seidel, D.; Leenders, F.; Ansén, S.; Ludwig, C.; Engel-Riedel, W.; Stoelben, E.; Wolf, J.; Goparju, C.; Thompson, K.; Winckler, W.; Kwiatkowski, D.; Johnson, B. E.; Jänne, P. A.; Miller, V. A.; Pao, W.; Travis, W. D.; Pass, H. I.; Gabriel, S. B.; Lander, E. S.; Thomas, R. K.; Garraway, L. A.; Getz, G.; Meyerson, M. Mapping the hallmarks of lung adenocarcinoma with massively parallel sequencing. *Cell* **2012**, *150* (6), 1107−1120.

(7) Peifer, M.; Fernández-Cuesta, L.; Sos, M. L.; George, J.; Seidel, D.; Kasper, L. H.; Plenker, D.; Leenders, F.; Sun, R.; Zander, T.; Menon, R.; Koker, M.; Dahmen, I.; Müller, C.; Di Cerbo, V.; Schildhaus, H. U.; Altmüller, J.; Baessmann, I.; Becker, C.; de Wilde, B.; Vandesompele, J.; Böhm, D.; Ansén, S.; Gabler, F.; Wilkening, I.; Heynck, S.; Heuckmann, J. M.; Lu, X.; Carter, S. L.; Cibulskis, K.; Banerji, S.; Getz, G.; Park, K. S.; Rauh, D.; Grütter, C.; Fischer, M.; Pasqualucci, L.; Wright, G.; Wainer, Z.; Russell, P.; Petersen, I.; Chen, Y.; Stoelben, E.; Ludwig, C.; Schnabel, P.; Hoffmann, H.; Muley, T.; Brockmann, M.; Engel-Riedel, W.; Muscarella, L. A.; Fazio, V. M.; Groen, H.; Timens, W.; Sietsma, H.; Thunnissen, E.; Smit, E.; Heideman, D. A.; Snijders, P. J.; Cappuzzo, F.; Ligorio, C.; Damiani, S.; Field, J.; Solberg, S.; Brustugun, O. T.; Lund-Iversen, M.; Sänger, J.; Clement, J. H.; Soltermann, A.; Moch, H.; Weder, W.; Solomon, B.; Soria, J. C.; Validire, P.; Besse, B.; Brambilla, E.; Brambilla, C.; Lantuejoul, S.; Lorimier, P.; Schneider, P. M.; Hallek, M.; Pao, W.; Meyerson, M.; Sage, J.; Shendure, J.; Schneider, R.; Büttner, R.; Wolf, J.; Nürnberg, P.; Perner, S.; Heukamp, L. C.; Burindle, P. K.; Haas, S.; Thomas, R. K. Integrative genome analyses identify key somatic driver mutations of small-cell lung cancer. *Nat. Genet.* **2012**, *44* (10), 1104−1110.

(8) Kikuchi, T.; Hassanein, M.; Amann, J. M.; Liu, Q.; Slebos, R. J.; Rahman, S. M.; Kaufman, J. M.; Zhang, X.; Hoeksema, M. D.; Harris, B. K.; Li, M.; Shyr, Y.; Gonzalez, A. L.; Zimmerman, L. J.; Liebler, D. C.; Massion, P. P.; Carbone, D. P. In-depth Proteomic Analysis of Nonsmall Cell Lung Cancer to Discover Molecular Targets and Candidate Biomarkers. *Mol. Cell. Proteomics* **2012**, *11* (10), 916−932.

(9) Eriksson, H.; Lengqvist, J.; Hedlund, J.; Uhlen, K.; Orre, L. M.; Bjellqvist, B.; Persson, B.; Lehtio, J.; Jakobsson, P. J. Quantitative membrane proteomics applying narrow range peptide isoelectric focusing for studies of small cell lung cancer resistance mechanisms. *Proteomics* **2008**, *8* (15), 3008−3018.

(10) Käll, L.; Canterbury, J. D.; Weston, J.; Noble, W. S.; MacCoss, M. J. Semi-supervised learning for peptide identification from shotgun proteomics datasets. *Nat. Methods* **2007**, *4* (11), 923−925.

(11) Spivak, M.; Weston, J.; Bottou, L.; Käll, L.; Noble, W. S. Improvements to the percolator algorithm for Peptide identification from shotgun proteomics data sets. *J. Proteome Res.* **2009**, *8* (7), 3737−3745.

(12) Reiter, L.; Claassen, M.; Schrimpf, S. P.; Jovanovic, M.; Schmidt, A.; Buhmann, J. M.; Hengartner, M. O.; Aebersold, R. Protein identification false discovery rates for very large proteomics data sets generated by tandem mass spectrometry. *Mol. Cell. Proteomics* **2009**, *8* (11), 2405−2417.

(13) Eriksson, L.; Antti, H.; Gottfries, J.; Holmes, E.; Johansson, E.; Lindgren, F.; Long, I.; Lundstedt, T.; Trygg, J.; Wold, S. Using chemometrics for navigating in the large data sets of genomics, proteomics, and metabonomics (gpm). *Anal. Bioanal. Chem.* **2004**, *380* (3), 419−429.

(14) Chong. Performance of some variable selection methods when multicollinearity is present. *Chemom. Intell. Lab. Syst.* **2005**, *78* (1−2), 103−112.

(15) Huang, d. w.; Sherman, B. T.; Lempicki, R. A. Systematic and integrative analysis of large gene lists using DAVID bioinformatics resources. *Nat. Protoc.* **2009**, *4* (1), 44−57.

(16) Herrero, J.; Valencia, A.; Dopazo, J. A hierarchical unsupervised growing neural network for clustering gene expression patterns. *Bioinformatics* **2001**, *17* (2), 126−136.

(17) Cuezva, J. M.; Krajewska, M.; de Heredia, M. L.; Krajewski, S.; Santamaria, G.; Kim, H.; Zapata, J. M.; Marusawa, H.; Chamorro, M.; Reed, J. C. The bioenergetic signature of cancer: a marker of tumor progression. *Cancer Res.* **2002**, *62* (22), 6674−6681.

(18) Hernlund, E.; Hjerpe, E.; Avall-Lundqvist, E.; Shoshan, M. Ovarian carcinoma cells with low levels of beta-F1-ATPase are sensitive to combined platinum and 2-deoxy-D-glucose treatment. *Mol. Cancer Ther.* **2009**, *8* (7), 1916−1923.

(19) De Petris, L.; Orre, L. M.; Kanter, L.; Pernemalm, M.; Koyi, H.; Lewensohn, R.; Lehtiö, J. Tumor expression of S100A6 correlates with survival of patients with stage I non-small-cell lung cancer. *Lung Cancer* **2009**, *63* (3), 410−417.
(20) Munksgaard Persson, M.; Johansson, M. E.; Monsef, N.; Planck, M.; Beckman, S.; Seckl, M. J.; Rönnstrand, L.; Påhlman, S.; Pettersson, H. M. HIF-2α expression is suppressed in SCLC cells, which survive in moderate and severe hypoxia when HIF-1α is repressed. *Am. J. Pathol.* **2012**, *180* (2), 494−504.
(21) Lopez-Rios, F.; Sanchez-Arago, M.; Garcia-Garcia, E.; Ortega, A. D.; Berrendero, J. R.; Pozo-Rodriguez, F.; Lopez-Encuentra, A.; Ballestin, C.; Cuezva, J. M. Loss of the mitochondrial bioenergetic capacity underlies the glucose avidity of carcinomas. *Cancer Res.* **2007**, *67* (19), 9013−9017.
(22) Denko, N. C. Hypoxia, HIF1 and glucose metabolism in the solid tumour. *Nat. Rev. Cancer* **2008**, *8* (9), 705−713.
(23) Wise, D. R.; DeBerardinis, R. J.; Mancuso, A.; Sayed, N.; Zhang, X. Y.; Pfeiffer, H. K.; Nissim, I.; Daikhin, E.; Yudkoff, M.; McMahon, S. B.; Thompson, C. B. Myc regulates a transcriptional program that stimulates mitochondrial glutaminolysis and leads to glutamine addiction. *Proc. Natl. Acad. Sci. U.S.A.* **2008**, *105* (48), 18782−18787.
(24) Cuezva, J. M.; Chen, G.; Alonso, A. M.; Isidoro, A.; Misek, D. E.; Hanash, S. M.; Beer, D. G. The bioenergetic signature of lung adenocarcinomas is a molecular marker of cancer diagnosis and prognosis. *Carcinogenesis* **2004**, *25* (7), 1157−1163.
(25) Keith, B.; Johnson, R. S.; Simon, M. C. HIF1α and HIF2α: sibling rivalry in hypoxic tumour growth and progression. *Nat. Rev. Cancer* **2012**, *12* (1), 9−22.
(26) Hung, J. J.; Yang, M. H.; Hsu, H. S.; Hsu, W. H.; Liu, J. S.; Wu, K. J. Prognostic significance of hypoxia-inducible factor-1alpha, TWIST1 and Snail expression in resectable non-small cell lung cancer. *Thorax* **2009**, *64* (12), 1082−1089.
(27) Kim, S. J.; Rabbani, Z. N.; Dewhirst, M. W.; Vujaskovic, Z.; Vollmer, R. T.; Schreiber, E. G.; Oosterwijk, E.; Kelley, M. J. Expression of HIF-1α, CA IX, VEGF, and MMP-9 in surgically resected non-small cell lung cancer. *Lung Cancer* **2005**, *49* (3), 325−335.
(28) Giatromanolaki, A.; Koukourakis, M. I.; Sivridis, E.; Turley, H.; Talks, K.; Pezzella, F.; Gatter, K. C.; Harris, A. L. Relation of hypoxia inducible factor 1 alpha and 2 alpha in operable non-small cell lung cancer to angiogenic/molecular profile of tumours and survival. *Br. J. Cancer* **2001**, *85* (6), 881−980.
(29) Cavailles, V.; Garcia, M.; Rochefort, H. Regulation of cathepsin-D and pS2 gene expression by growth factors in MCF7 human breast cancer cells. *Mol. Endocrinol.* **1989**, *3* (3), 552−558.
(30) Krishnamachary, B.; Berg-Dixon, S.; Kelly, B.; Agani, F.; Feldser, D.; Ferreira, G.; Iyer, N.; LaRusch, J.; Pak, B.; Taghavi, P.; Semenza, G. L. Regulation of colon carcinoma cell invasion by hypoxia-inducible factor 1. *Cancer Res.* **2003**, *63* (5), 1138−1143.
(31) Zaidi, N.; Maurer, A.; Nieke, S.; Kalbacher, H. Cathepsin D: a cellular roadmap. *Biochem. Biophys. Res. Commun.* **2008**, *376* (1), 5−9.
(32) Koblinski, J. E.; Ahram, M.; Sloane, B. F. Unraveling the role of proteases in cancer. *Clin. Chim. Acta* **2000**, *291* (2), 113−135.
(33) Schwartz, M. K. Tissue cathepsins as tumor markers. *Clin. Chim. Acta* **1995**, *237* (1−2), 67−78.
(34) Ohri, S. S.; Vashishta, A.; Vetvickova, J.; Fusek, M.; Vetvicka, V. Procathepsin D expression correlates with invasive and metastatic phenotype of MDA-MB-231 derived cell lines. *Int. J. Biol. Macromol.* **2007**, *41* (2), 204−209.
(35) Sudhir, P. R.; Chen, C. H.; Pavana Kumari, M.; Wang, M. J.; Tsou, C. C.; Sung, T. Y.; Chen, J. Y. Label-free quantitative proteomics and N-glycoproteomics analysis of KRAS-activated human bronchial epithelial cells. *Mol. Cell. Proteomics* **2012**, *11* (10), 901−915.
(36) Mimae, T.; Tsuta, K.; Maeshima, A. M.; Okada, M.; Asamura, H.; Kondo, T.; Tsuda, H. Cathepsin D as a potential prognostic marker for lung adenocarcinoma. *Pathol., Res. Pract.* **2012**, *208* (9), 534−540.
(37) Semenza, G. L.; Jiang, B. H.; Leung, S. W.; Passantino, R.; Concordet, J. P.; Maire, P.; Giallongo, A. Hypoxia response elements in the aldolase A, enolase 1, and lactate dehydrogenase A gene promoters contain essential binding sites for hypoxia-inducible factor 1. *J. Biol. Chem.* **1996**, *271* (51), 32529−32537.
(38) Altenberg, B.; Greulich, K. O. Genes of glycolysis are ubiquitously overexpressed in 24 cancer classes. *Genomics* **2004**, *84* (6), 1014−1020.
(39) Shoshan-Barmatz, V.; Keinan, N.; Zaid, H. Uncovering the role of VDAC in the regulation of cell life and death. *J. Bioenerg. Biomembr.* **2008**, *40* (3), 183−191.
(40) Brahimi-Horn, M. C.; Ben-Hail, D.; Ilie, M.; Gounon, P.; Rouleau, M.; Hofman, V.; Doyen, J.; Mari, B.; Shoshan-Barmatz, V.; Hofman, P.; Pouysségur, J.; Mazure, N. M. Expression of a Truncated Active Form of VDAC1 in Lung Cancer Associates with Hypoxic Cell Survival and Correlates with Progression to Chemotherapy Resistance. *Cancer Res.* **2012**, *72* (8), 2140−2150.
(41) Azoulay-Zohar, H.; Israelson, A.; Abu-Hamad, S.; Shoshan-Barmatz, V. In self-defence: hexokinase promotes voltage-dependent anion channel closure and prevents mitochondria-mediated apoptotic cell death. *Biochem. J.* **2004**, *377* (Pt2), 347−355.
(42) Shoshan-Barmatz, V.; Ben-Hail, D. VDAC, a multi-functional mitochondrial protein as a pharmacological target. *Mitochondrion* **2012**, *12* (1), 24−34.
(43) Memmott, R. M.; Mercado, J. R.; Maier, C. R.; Kawabata, S.; Fox, S. D.; Dennis, P. A. Metformin prevents tobacco carcinogen–induced lung tumorigenesis. *Cancer Prev. Res.* **2010**, *3* (9), 1066−1076.
(44) Lee, C.; Raffaghello, L.; Brandhorst, S.; Safdie, F. M.; Bianchi, G.; Martin-Montalvo, A.; Pistoia, V.; Wei, M.; Hwang, S.; Merlino, A.; Emionite, L.; de Cabo, R.; Longo, V. D. Fasting cycles retard growth of tumors and sensitize a range of cancer cell types to chemotherapy. *Sci. Transl. Med.* **2012**, *4* (124), 124ra27.
(45) Schulze, A.; Harris, A. L. How cancer metabolism is tuned for proliferation and vulnerable to disruption. *Nature* **2012**, *491* (7424), 364−373.